Journal of Materials Chemistry

Cite this: J. Mater. Chem., 2012, 22, 2111

www.rsc.org/materials

PAPER

Rapid mineralization of porous gelatin scaffolds by electrodeposition for bone tissue engineering

Chuanglong He,*[abc] Fan Zhang,[b] Lijun Cao,[b] Wei Feng,[b] Kexin Qiu,[b] Yanzhong Zhang,[b] Hongsheng Wang,[b] Xiumei Mo[b] and Jinwu Wang*[d]

Received 17th September 2011, Accepted 28th October 2011
DOI: 10.1039/c1jm14631a

In bone tissue engineering, rapid mineralization of polymeric scaffolds is of particular importance in protecting the encapsulated therapeutic drugs or growth factors from loss and degradation. Here, we present a simple and rapid approach to the fabrication of mineralized porous scaffolds for bone tissue engineering. In this approach, three-dimensional (3-D) porous gelatin scaffolds were firstly fabricated by freeze-drying followed by an electrodeposition process for mineralization. We show that a high-quality apatite coating on the gelatin scaffold could be achieved within a couple of hours by electrodeposition. Increasing the deposition voltage or electrolyte temperature favored to the formation of large amounts of apatite coatings with compositions dominated by the hydroxyapatite crystals, whereas the presence of ultrasonic field facilitated the production of homogeneous apatite coatings. Moreover, biological assays indicated that the mineralized scaffolds exhibited better support for the proliferation and osteoblastic differentiation of MC3T3-E1 cells over a neat gelatin scaffold, especially for the case of mineralized scaffolds by electrodeposition at 60 °C. Therefore, the method developed would be highly desired for the rapid mineralization of polymer scaffolds in which biological molecules were loaded for functional bone tissue engineering applications.

Introduction

It is well known that bone is a natural inorganic–organic nanocomposite, in which the inorganic hydroxyapatite (HAp) nanocrystals and the organic collagen fibrils are well compounded and organized into a highly complex and hierarchical architecture.[1–3] Thus, from a biomimetic point of view it has been a rational choice to use a polymer-based composite approach for constructing bone tissue scaffolds in tissue engineering research. Numerous studies have demonstrated that such minerals-incorporated scaffolds may play crucial roles in regulating cellular growth, differentiation, mineral deposition, and bone formation.[4–6]

Several approaches have been employed for the preparation of polymer/ceramic composite scaffolds including direct blending of mineral crystals with polymeric matrices,[7] co-precipitation,[8] and biomimetic mineralization by immersing polymeric matrices into a simulated body fluid (SBF).[9] Among them, biomimetic mineralization is regarded as the most effective due to its ability in producing materials with morphologies and structures resembling the natural bone.[10] However, mineralization by using SBF is time-consuming, and usually takes many more days to achieve an appropriate apatite coating.[11,12] This will probably give rise to the problems of polymer degradation and loss of the encapsulated therapeutic agents or growth factors if any, prior to their clinical applications.[13] Therefore, developing alternative and effective methods to realize rapid mineralization of bone tissue engineering scaffolds becomes clearly necessary.

Aimed at improving the surface bioactivity and bone-binding ability, electrodeposition (ED) has traditionally been used as an effective approach to deposit apatite coatings onto those metallic substrates.[14,15] Nevertheless, it has rarely been attempted for the mineralization of a biodegradable cellular scaffold. In a previous study,[13] we demonstrated that a uniform apatite coating with tunable topography and chemical composition could be rapidly deposited onto the surface of the nanofibers by altering the processing parameters during electrodeposition. However, given the situation that practical application of electrospun nanofibers in tissue regeneration is still a huge challenge due to their difficulty in three-dimensional (3-D) shaping and macroporous scaffolding,[12,16] the use of the electrodeposition technique for mineralizing conventional 3-D porous polymer scaffolds might result in suitable substitutes for practical bone tissue engineering.

[a]State Key Laboratory for Modification of Chemical Fibers and Polymer Materials, Donghua University, Shanghai, 201620, People's Republic of China
[b]College of Chemistry, Chemical Engineering and Biotechnology, Donghua University, Shanghai, 201620, People's Republic of China. E-mail: hcl@dhu.edu.cn
[c]Key Laboratory of Textile Science and Technology, Ministry of Education, Shanghai, 201620, People's Republic of China
[d]Department of Orthopaedic Surgery, Ninth People's Hospital, Shanghai Jiao Tong University School of Medicine, Shanghai, 200011, People's Republic of China

The aim of the present study is to fabricate mineralized porous scaffolds by combining the freeze-drying formation of porous scaffolds with subsequent electrodeposition. We first focused on the influence of different processing parameters including deposition voltage, temperature and ultrasonic field on the surface morphology, crystal structure and chemical composition of the mineralized scaffolds. Then, the effect of apatite coating properties on *in vitro* cellular functions, such as cell morphology, viability, alkaline phosphatase (ALP) activity and osteocalcin (OCN) expression, were evaluated using the MC3T3-E1 mouse pre-osteoblast cell.

Experimental

Materials

Gelatin powder from bovine skin (Type B, Approx 250 Bloom) and ascorbic acid were purchased from Sigma-Aldrich (Shanghai) Trading Co., Ltd (Shanghai, China). 1-Ethyl-3-(3-dimethylaminopropyl)carbodiimide hydrochloride (EDC) was obtained from Shanghai Medpep Co., Ltd. (Shanghai, China). $Ca(NO_3)_2 \cdot 4H_2O$ and $NH_4H_2PO_4$ were purchased from Shanghai Aibi Chemistry Preparation Co., Ltd. (Shanghai, China). All of the materials and solvents were used without further purification.

For cell culture, the MC3T3-E1 cell line was obtained from the Institute of Biochemistry and Cell Biology of the Chinese Academy of Sciences (Shanghai, China). Calcium- and magnesium-free phosphate buffered saline (PBS), fetal bovine serum (FBS), penicillin-streptomycin, trypsin and α-modified Eagle's medium (α-MEM) were obtained from Gibco Life Technologies Co. (Carlsbad, California). Dimethyl sulfoxide (DMSO) and 25% glutaraldehyde were purchased from China National Medicines Co., Ltd (Beijing, China). β-Glycerol phosphate was purchased from TCI (Shanghai) Development Co., Ltd. (Shanghai, China).

Preparation of 3-D porous scaffolds

Porous gelatin scaffolds were fabricated as previously reported.[17] Briefly, an aqueous solution of gelatin (5 w/v%) was prepared by dissolving gelatin in deionized water at 40 °C. Then, the homogeneous solution was injected into Teflon molds and immediately transferred into a freezer at −80 °C. The frozen mixtures were lyophilized within a freeze-dryer (Chris, Alpha 1-2LD, Germany) under vacuum for 48 h. The lyophilized gelatin scaffolds were then immersed in 50 mmol L^{-1} EDC/95% alcohol for cross-linking at 4 °C for 24 h. The cross-linked scaffolds were washed three times with deionized water to remove residual EDC. Finally, the scaffolds were freeze-dried again under the same conditions. The dried gelatin scaffolds were cut into samples with a size of 15 mm diameter and 2 mm thickness. All the samples were kept in a vacuum drying oven for further testing or cell culture.

Electrodeposition

Electrodeposition was performed under potentiostatic conditions in a two-electrode system (Fig. 1a). The dried gelatin porous scaffolds as shown in Fig. 1b–c were fixed on the surface of a stainless steel electrode (40 mm × 40 mm × 0.1 mm) by conducting adhesive, which served as the working electrode (cathode), and a platinum plate electrode with the same size was used as the counter electrode (anode). The electrolyte solution was consisted of 4.2×10^{-2} mol L^{-1} of $Ca(NO_3)_2 \cdot 4H_2O$ and 2.5×10^{-2} mol L^{-1} of $NH_4H_2PO_4$, with the Ca/P ratio equivalent to 1.67. The pH value was adjusted to 4.80 by $NH_3 \cdot H_2O$ and HCl.

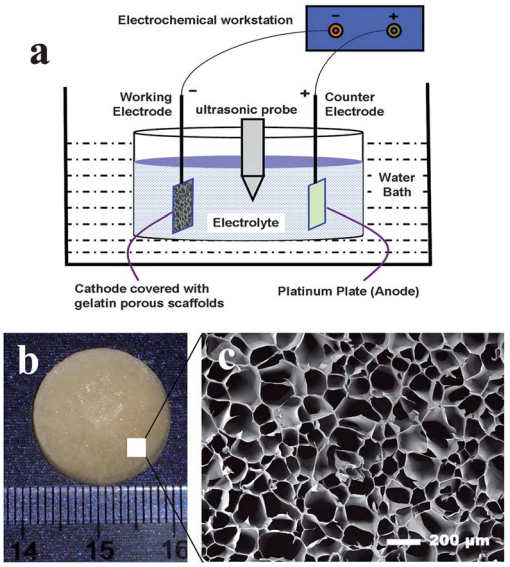

Fig. 1 (a) Schematic setup for the mineralization of porous gelatin scaffolds by electrodeposition. (b) The digital photo and (c) SEM micrograph of 3-D porous gelatin scaffold fabricated by the freeze-drying method.

Both electrodes were put into a 250 mL beaker containing 200 mL electrolyte solution, and the distance between the two electrodes was 2.5 cm. The setup was immersed in a thermostatic water bath to maintain the desired temperature (25, 37 or 60 °C). The deposition voltage used was 2 V, 3 V, or 5 V, controlled by a CHI600D electrochemistry workstation (Shanghai Chenhua Yi Qi Ltd). An ultrasonic probe was set at the middle of the two electrode plates to supply an ultrasonic environment, working with a power of 20 W and an interval of 6 s. After coating, the specimens were rinsed in deionized water to remove residual electrolyte, and dried in a vacuum drying oven for further use.

Characterization of the mineralized scaffolds

The morphology of the gelatin porous scaffolds before and after electrodeposition was observed using a scanning electron microscope (SEM, Hitachi TM-1000, Japan). The chemical composition of samples was analyzed by Fourier transform infrared spectroscopy (FTIR, Thermo Nicolet-670, USA). The crystalline phase of the deposits was characterized using an X-ray diffractometer (XRD, Rigaku, Japan) within the scanning region of $2\theta = 5$–$50°$, with Cu-Kα radiation at 40 kV and 40 mA. Prior to XRD analysis, the mineralized scaffolds were treated by ultrasonic separation to obtain the deposits, and then the apatite powders were dried in a vacuum oven. X-Ray photoelectron spectroscopy (XPS) spectra were recorded on a Kratos spectrometer (XSAM800, UK) with Al Kα radiation (1486.6 eV) at 12 kV and 15 mA. Samples were attached to the aluminium

sample platform with double-sided tape. The take-off angle was 30° with respect to sample plane. The Ca/P atomic ratio was then calculated to determine the chemical composition of the deposits.

Cell culture and seeding

The thawed MC3T3-E1 pre-osteoblasts in α-MEM supplemented with 10% FBS, containing 100 μg mL^{-1} penicillin and 100 μg mL^{-1} streptomycin were cultured in a humidified atmosphere of 5% CO_2 at 37 °C. For cell seeding, the dried gelatin porous scaffolds were placed in a 24-well plate and pressed with stainless steel rings. Prior to seeding with cells, the samples were sterilized under UV light for 2 h, and then immersed in 75% alcohol solution overnight. Afterwards, the sterile specimens were washed thrice with PBS for 30 min each, and twice with a complete medium (α-MEM, 10% FBS, 100 μg mL^{-1} penicillin and 100 μg mL^{-1} streptomycin) for 1 h each.

Cell proliferation and morphology

For cell proliferation assay, 2×10^4 cells were seeded on scaffolds in 48-well tissue culture plates. Cell proliferation was assessed by 3-[4,5-dimethylthiazol-2-yl]-2,5-diphenyltetrazolium bromide (MTT) after 1, 3, 5 and 7 days of cell culture. At the predetermined time point, culture medium was aspirated and the cell-scaffold construct was washed with PBS. Then 500 μL of culture medium containing 50 μL of MTT solution was added. After incubation at 37 °C for 1 h, the absorbance was measured at 490 nm on the plate reader (MK3, Thermo, USA).

Cell morphology after 3, 7 and 14 days of culture were observed by SEM (Hitachi TM-1000, Japan). Cell-scaffold constructs were washed with PBS and then fixed with 4% glutaraldehyde at 4 °C for 4 h. The constructs were then dehydrated in a graded series of ethanol solutions (30, 50, 75, 90, and 100%) and dried under vacuum. Afterwards, the constructs were sputter coated with gold and examined using SEM at an accelerating voltage of 15 kV.

ALP activity

For ALP and subsequent OCN assay, 2×10^4 cells were seeded on each scaffold in a 24-well tissue culture plate. An osteogenic medium, which consisted of complete medium supplemented with 50 mg mL^{-1} ascorbic acid and 10 mmol L^{-1} β-glycerol phosphate, was added after 24 h of cell seeding. The medium was changed every other day. ALP activity was measured using the cell lysates after 3, 7 and 14 days of cell seeding. At each culturing period, the cell-grown scaffolds were removed and washed twice with PBS and stored at −80 °C. After freeze-drying, the samples were cut down with scissors, followed by adding a cell lysis buffer containing 0.2% Triton-X 100 to the samples. The cell lysate was frozen at −20 °C prior to measurement. The ALP activity of the cell lysate was detected using a mouse BALP ELISA kit from RapidBio (RapidBio Laboratory, USA). The assay was performed according to the manufacturer's instructions and the absorbance at 450 nm was measured on the plate reader. The ALP content is expressed as a ratio of ALP/cell (ng $cell^{-1}$).

OCN content

OCN content was measured in the culture medium using the mouse BGP/OCN ELISA kit (RapidBio Laboratory, USA). In brief, culture medium was removed from each well after 3, 7 and 14 days of culture and stored at −20 °C until the final measurement. Samples were diluted 100× with sterile filtered Millipore water to achieve concentrations within the detection range of the assay. Mouse OCN standards were diluted similarly to final concentrations of 0–80 ng mL^{-1}. Then, 50 μL of standard or sample was added to the 96-well plate for the absorbance measurement at 450 nm on the plate reader according to the manufacturer's protocol. OCN content is expressed as a ratio of OCN/cell (ng $cell^{-1}$).

Statistical analysis

All experiments were conducted at least three times and data were reported as the mean ± standard deviation (SD). Statistical analysis of data was performed by using the Student's *t*-test, and the statistical difference between two sets of data was considered when $p < 0.05$.

Results and discussion

Influence of deposition duration

Fig. 2 shows the SEM micrographs of mineralized gelatin scaffolds deposited at 37 °C and 3 V for varied deposition durations. After 1 h, the deposited crystals were well distributed on the surface of the scaffold pore walls (Fig. 2a and 2d). When the mineralization time was increased to 2 h, the spherical and nest-like crystal formed, especially on the edge of the pore wall (Fig. 2b and 2e). The surface of the scaffold was fully covered with the mineral within 2 h of deposition. With a further lengthening the deposition time to 3 h, even more spherical and nest-like crystals were formed due to the continuous formation of new nuclei and crystalline growth (Fig. 2c and 2f). Clearly, the electrodeposition process enabled a significantly shortened time in scaffold mineralization, which is more advantageous for minimizing polymer degradation and loss of the encapsulated therapeutic agents or growth factors during the long-term incubation, if incorporated for functional delivery.

Influence of deposition voltage

The deposition potential is a key factor that influenced the topography and mass production of the deposits. A plate-like mineral coating was formed along the top of the pores of the gelatin scaffold under a low voltage of 2 V at 37 °C for 2 h (Fig. 3a and 3d). When the deposition voltage increased to 3 V, it gave rise to a uniform and nest-like coating (Fig. 3b and 3e). A further increase of the voltage to 5 V resulted in the formation of a fine and well-distributed coating on the outer pore surfaces of the scaffold (Fig. 3c and 3f). On the other hand, the mass of the scaffolds also increased with using higher deposition voltages. For example, the mass increase for the scaffold deposited at 2 V was about 2.4 ± 2%, whereas the values increased to 12.0 ± 7% at 3 V and 18.1 ± 7% at 5 V respectively.

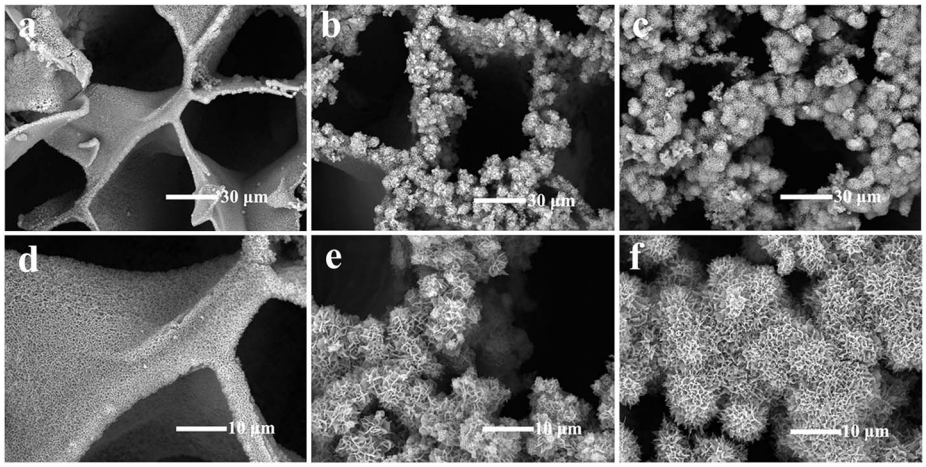

Fig. 2 SEM images of mineralized gelatin scaffolds prepared by electrodeposition at 37 °C and 3 V for (a) 1 h, (b) 2 h, (c) 3 h; (d), (e), and (f) are the amplified images of (a), (b), and (c), respectively.

Fig. 3h presents the X-ray diffraction (XRD) patterns of the minerals deposited on the surface of the gelatin scaffolds under different deposition voltages at 37 °C for 2 h. At a lower deposition voltage of 2 V, well-defined (020), (021), and (041) peaks were observed, which matched well with the crystalline data (the JCPDS card 09-0077) for the calcium phosphate dihydrate (DCPD), suggesting the nature of the major crystal structure. However, when the deposition voltages was increased to 3 V and 5 V, the XRD patterns of the deposited crystals showed some new peaks which correspond to the reflections from the HAp (002), (211), and (300) diffraction planes (JCPDS card 09-0432). Evidently, the higher deposition voltage could result in some deposited crystals being converted from DCPD to HA. This is also coincided with our previous study.[13]

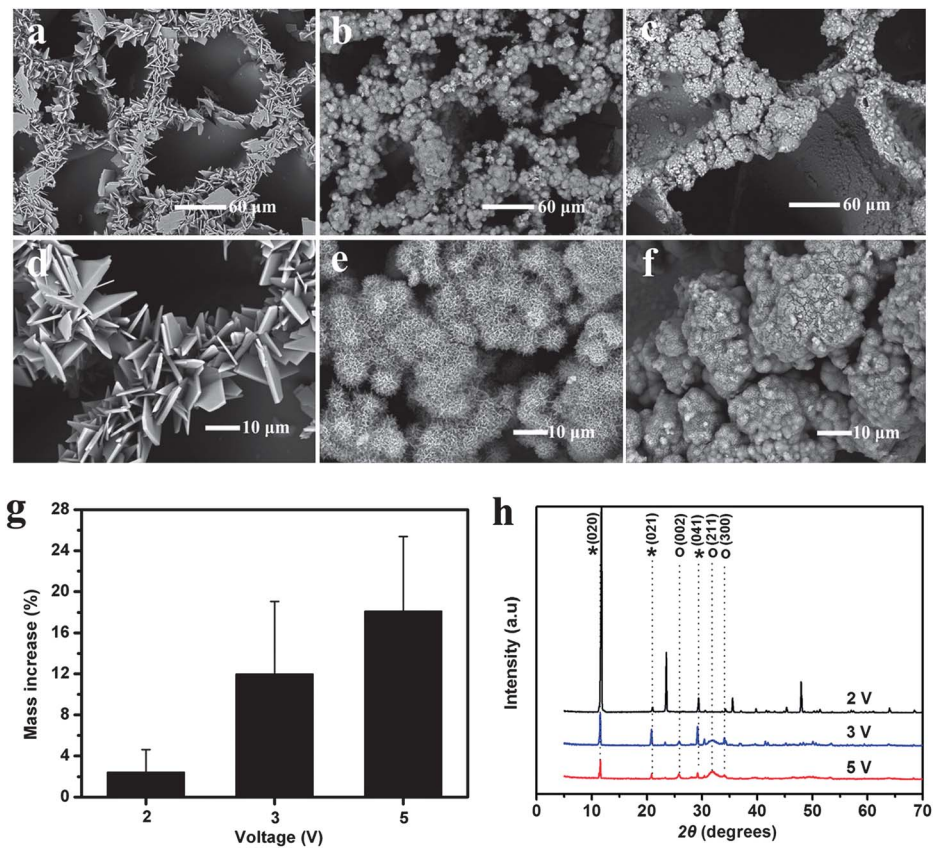

Fig. 3 (a)–(f) SEM images of gelatin scaffolds obtained at 37 °C for 3 h under different deposition voltage: (a) 2 V, (b) 3 V, (c) 5 V; (d), (e), and (f) are the amplified images of (a), (b), and (c), respectively; (g) mass increase of gelatin scaffolds processed under different voltages (2, 3, and 5 V) at 37 °C for 3 h; (h) XRD patterns taken from gelatin scaffolds after electrodeposition for 3 h at 37 °C under different voltages (2, 3, and 5 V, * = DCPD, ○ = HA).

Influence of deposition temperature

Fig. 4a–b shows the SEM images of the apatite coating obtained at different electrolyte temperature (25 °C and 60 °C) at 3 V for 2 h. The morphology of the deposits varied remarkably with the electrolyte temperatures. The coating obtained at 25 °C was plate-like, similar to that deposited at 2 V and 37 °C (Fig. 3a and 3d). At 60 °C, the mineral crystals were needle-like, close to the HAp phase in human bone tissue.[18] Moreover, it was found that increasing the electrolyte temperature also led to a high amount of mineral deposition. For instance, under the same potential of 3 V for 2 h, the mass increase of gelatin scaffolds obtained at 25 °C was merely 5.4 ± 5.0%. When the temperature increased to 37 °C and 60 °C, the mass increases were 12.0 ± 6.9% and 15.3 ± 6.2%, respectively (Fig. 4c).

XRD patterns (Fig. 4d) were obtained to detect the crystalline structure of the minerals deposited at different temperatures (25, 37 and 60 °C). The peaks for DCPD and HAp were observed at 2θ = 11.7°, 20.8°, 29.2°, and 25.8°, 31.6°, 34.0°, respectively, indicating a multi-phasic but discernable crystalline apatite varying with the electrodeposition temperature. While the DCPD and HAp peaks could be seen obviously in the patterns of mineral crystals deposited at 25 °C and 60 °C, respectively, both of them could be observed for that of the sample deposited at 37 °C. The results are in accordance with our previous study, and suggest that the high temperature drove a conversion from DCPD to HA.[13] Furthermore, typical XPS survey spectra (Fig. 4e) shows that the bands for O 1s, C 1s, Ca 2s, Ca 2p, Ca 3s, Ca 3p, P 2s and P 2p are all presented similarly for the three kinds of apatite crystals. However, their Ca/P molar ratio varied as follows: 1.11 (25 °C), 1.20 (37 °C) and 1.30 (60 °C). Meanwhile, the peaks of Ca 2p are located at about 347.0 eV, suggesting a bonding between the calcium atom and the phosphate group (PO_4^{3-}).[20] In general, the Ca/P molar ratio of calcium phosphates is an important parameter to affect their thermostability, solubility and biocompatibility, which is 1.0 in DCPD, 1.33 in octacalcium phosphate (OCP), 1.5 in tricalcium phosphate

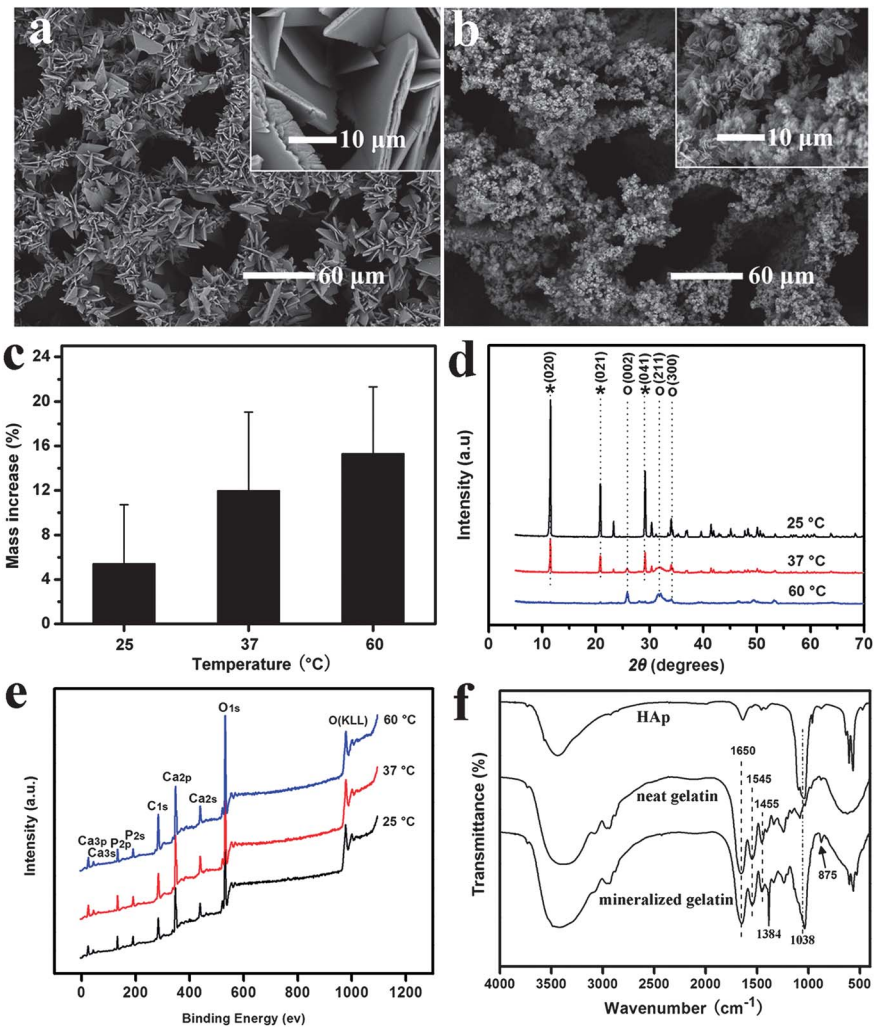

Fig. 4 (a,b) SEM images of gelatin scaffolds obtained under 3 V for 2 h at different temperatures, the inset images are the amplified ones: (a) 25 °C, (b) 60 °C; (c) mass increase of gelatin scaffolds processed under 3 V for 2 h at different temperatures (25 and 60 °C); (d) XRD patterns taken from gelatin scaffolds after electrodeposition for 2 h at different temperatures (25, 37, and 60 °C, * = DCPD, ○ = HA); (e) XPS spectra of the apatite crystals obtained at various temperatures at 3 V for 2 h; (f) FTIR spectra of commercial HAp crystals, neat gelatin scaffolds and mineralized scaffolds which were obtained at 60 °C under 3 V for 2 h by electrodeposition.

(TCP) and 1.67 in stoichiometric hydroxyapatite.[3] The molar ratio of the Ca/P in the present apatite coatings varies from 1.11 to 1.30, indicating that the present coatings contain different calcium phosphate compounds.

Fig. 4f shows FTIR spectra of commercial HAp crystals, neat gelatin scaffold and mineralized scaffold by electrodeposition at 60 °C and 3 V for 2 h. The commercial HAp spectrum shows the characteristic peaks of the phosphate absorption bands at 1038 cm^{-1} for the P–O stretch, and 564 cm^{-1} and 602 cm^{-1} for a P–O stretch coupled with a P–O bend.[19] For the spectrum of the neat gelatin scaffold, the peaks at 1650 cm^{-1} and 1545 cm^{-1} corresponding to amide I for the C=O stretching vibration and amide II for the N–H bending vibration were identified, together with the peak at 1455 cm^{-1} are assigned to the ester band for the C–O stretch. Moreover, the presence of the bands at 1384 cm^{-1} and 875 cm^{-1}, which are attributed to the carbonate groups, would suggest the formation of a carbonated calcium phosphate during the electrodeposition process. This is similar to the one found in bone apatite.[21]

Influence of ultrasound

Fig. 5a–b shows the SEM images of mineralized gelatin scaffolds obtained at 37 °C and 3 V for 2 h in the absence/presence of ultrasound (20 W), which was found to affect the homogeneity of the apatite coatings. For example, the coating obtained in the absence of ultrasound shows an uneven surface. By contrast, the ultrasonic electrodeposition formed a homogenous coating layer on the surface of the pore walls. XRD analysis (Fig. 5c) indicates that there is no significant difference in the main diffraction peaks for the mineral crystals with and without the ultrasonic field. The only discrimination is that the crystals obtained in the presence of ultrasound showed better crystallinity as higher intensity reflection planes are discernable.

Proposed mechanism of electrodeposition

It is generally accepted that the electrodeposition on metallic substrates involves electrochemical reactions, acid–base reactions and precipitation reactions.[15] The electrochemical reactions on the cathode surface result in an elevated pH environment mainly due to the reduction of water. This invokes the supersaturation of calcium phosphate salts at the vicinity of the cathode where different calcium phosphates, including HAp, OCP, TCP and DCPD, may be deposited onto the cathode.[15,22] Additionally, there are evidences supporting that organic macromolecules with molecular recognition also regulate the growth of Ca–P crystals.[23–25]

Gelatin is an amphoteric macromolecule with polar head-groups on the surface such as –COOH, –OH, and $–NH_2$.[26] The –COOH groups existing on the surface of the scaffolds are in the form of $–COO^-$ when the pH of solution is greater than the isoelectric point (IEP) of gelatin. These carboxyl ions (COO^-) as the active groups promote the binding of positive ions from the solution to the substrate, thus triggering the nucleation of inorganic crystals.[25,27] As schematically illustrated in Fig. 6, when a deposition voltage is applied, the pH value in the vicinity of the cathode will increase, which results in the gelatin macromolecules being negatively charged. Meanwhile, the calcium ions in the electrolyte will migrate to the vicinity of the cathode, thus

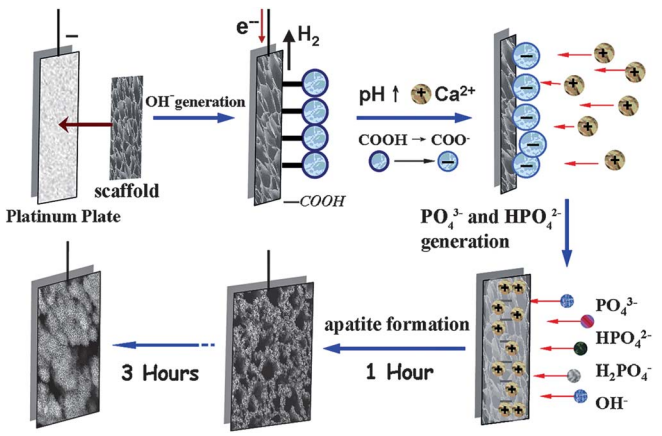

Fig. 6 Schematic illustration of a hypothesized mechanism for the generation of calcium phosphate crystals during the electrodeposition. When a deposition voltage is applied, the pH value in the vicinity of electrode increases, and the amphiprotic gelatin macromolecules on the surface of the scaffolds were negatively charged. Firstly, the Ca^{2+} in the electrolyte migrated to the cathode, and then the anions around the cathode, including PO_4^{3-}, HPO_4^{2-}, $H_2PO_4^-$ and OH^-, combined with Ca^{2+} to form various Ca–P deposits onto the surface of porous scaffolds. Further increase of deposition time leads to the growth of nuclei and larger apatite crystals.

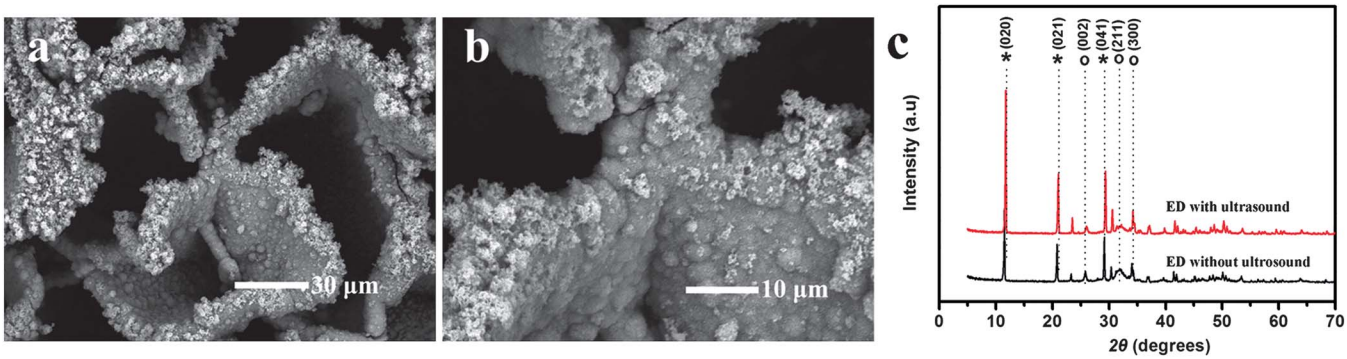

Fig. 5 (a) SEM image of gelatin scaffolds processed at 3 V and 37 °C for 2 h with ultrasonic process (20 W), (b) amplified images of (a); (c) XRD patterns taken from gelatin scaffolds after electrodeposition at 3 V and 37 °C for 2 h (with and without ultrasonic process, * = DCPD, ○ = HA).

different Ca–P crystals will deposit onto the surface of the porous gelatin scaffolds depending on their thermodynamic stability in solution.[28] A higher deposition voltage affects the current density distribution on the electrodes, which generally results in more drastic electrochemical reactions by producing a high supersaturation condition in the vicinity of the gelatin scaffold. This consequently promotes the heterogeneous nucleation of calcium phosphate and forms a dense and uniform apatite layer on the surface of the scaffold. The electrolyte temperature is another governing factor since thermodynamic conditions such as the dissociation constant of phosphoric acid and water, the activity coefficients of ions, and the solubility products of calcium phosphates are affected under different electrolyte temperatures. However, the final deposits formed represent the most thermodynamically stable mineral crystals according to the classical theory of free energy change in supersaturated solutions.[28] The solubility product of HAp decreases as the temperature increases, and thereby the elevated temperature facilitates the precipitation of HAp.[15] Additionally, the use of ultrasonic field in electrodeposition can accelerate the nucleation and growth of crystals by increasing the stirring of the electrolyte, making the formed deposits more homogeneous.[29,30]

Cell morphology on different gelatin scaffolds

As is well-known, both the chemical composition and topography of mineral deposition are important mediating factors for the adhesion, proliferation and differentiation of bone cells and bone regeneration.[31,32] We hypothesized that the formed apatite coating on the surface of the gelatin scaffold would encourage the osteogenic capacity of mouse MC3T3-E1 pre-osteoblast cells to differentiate into osteoblastic phenotypes.[33,34] Such a verification was performed based on the mineralized scaffolds prepared under 3 V for 2 h with different electrolyte temperatures, in comparison with the neat gelatin scaffolds.

Fig. 7 shows pre-osteoblast morphology on a neat gelatin scaffold (Fig.7 a–c) and a mineralized gelatin scaffold (Fig.7 d–f) after 3, 7 and 14 days of culture. At day 3, the MC3T3-E1 presented a round shape on both scaffolds, and became elongated and spindle-like after 7 days of culture. At day 14, cells adopted a polygonal morphology and spread well on all the scaffolds, and were observed to span across the pore cavity in the neat gelatin scaffold (Fig. 7c). The results suggest that MC3T3-E1 cells are able to grow and proliferate well on neat and mineralized gelatin scaffolds.

Cell proliferation

MTT assay results are shown in Fig. 8a. No significant differences in cell proliferation were observed among all the scaffolds at days 3 and 5. Nevertheless, the apatite-coated scaffolds exhibited greater cell growth than that of the neat gelatin scaffold, especially for the mineralized scaffold deposited at 60 °C ($p < 0.05$), and the difference became even more distinct ($p < 0.01$) at day 14. Comparing the mineralized scaffolds with different apatite contents, the scaffold obtained at 60 °C shows significantly greater cell proliferation than the scaffold obtained at 25 °C. These results indicate that the apatite-coated scaffolds seem to facilitate the cell proliferation, and the mineralized scaffold with a higher apatite content supported better the cell growth.

ALP activity

Osteogenic differentiation of osteoblast-like cells seeded on scaffolds is of paramount importance for successful bone regeneration, and ALP activity is regarded as an early marker of osteoblast differentiation.[35] To evaluate the influences of the deposited apatite contents on the osteogenic differentiation of MC3T3-E1 cells, the ALP activity of the cells was examined at days 3, 7, and 14. As shown in Fig. 8b, the ALP activity on all scaffolds increases remarkably with culture time during the 14 day culture period. All the mineralized scaffolds exhibit the higher ALP activity than that of the neat gelatin scaffold, especially for the scaffold obtained at 60 °C, showing significant differences at days 7 ($p < 0.05$) and 14 ($p < 0.01$). For different mineralized scaffolds, the increases in cell ALP activity were

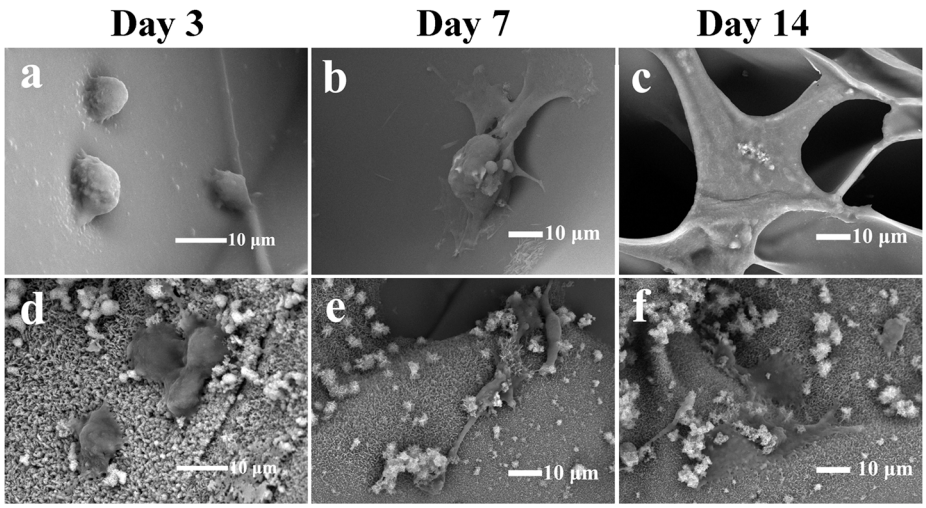

Fig. 7 SEM images of MC3T3-E1 morphology on neat gelatin scaffolds and mineralized scaffolds (obtained at 37 °C, 3 V for 2 h) for 3, 7, and 14 days. Cells cultured on neat gelatin scaffolds for (a) 3 days, (b) 7 days, and (c) 14 days; and on mineralized scaffolds for (d) 3 days, (e) 7 days, and (f) 14 days.

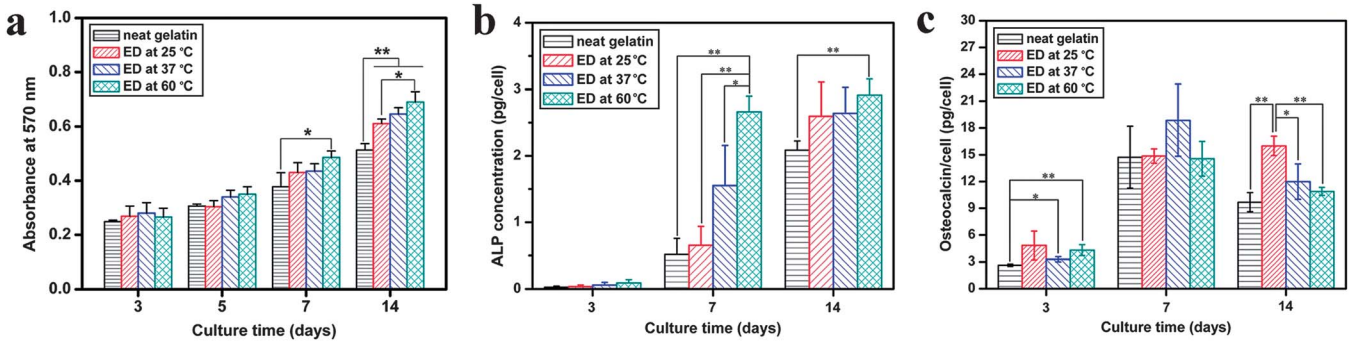

Fig. 8 (a) Relative proliferation rate (b) ALP activity, and (c) OCN protein content of MC3T3-E1 cells cultured on the neat gelatin scaffold and the mineralized gelatin scaffolds after culturing for up to 14 days. The mineralized scaffolds were fabricated by electrodeposition under 3 V for 2 h at 25, 37, and 60 °C, respectively. Significant difference between groups is indicated (*$p < 0.05$; **$p < 0.01$).

observed on the scaffolds prepared at higher electrolyte temperature. On day 7, the scaffold obtained at 60 °C demonstrated the significant higher ALP activity than the scaffolds obtained at 37 °C ($p < 0.05$) and 25 °C ($p < 0.01$).

The MC3T3-E1 cells grown on the mineralized scaffolds showed higher levels of ALP activity than that on the neat gelatin scaffold at days 7 and 14, proving the enhanced effects of apatite-coated scaffolds on the osteogenic differentiation of MC3T3-E1 cells. The results obtained here are also in good agreement with previous studies[7,36,37] Moreover, it was noticed that mineralized scaffolds prepared at higher electrolyte temperature resulted in increased ALP activity. This may be due to the fact that apatite quantities deposited are associated with the electrolyte temperatures during the electrodeposition process, also implying that a higher apatite content could provide a more effective substrate for cellular differentiation.

OCN content

OCN is a bone-specific protein which is often considered as a late-stage marker of osteoblastic differentiation.[34] Fig. 8c shows the content of OCN protein detected in cell culture media for mineralized and neat gelatin scaffolds using an enzymatic immunoassay. On day 3, although lower expression of OCN levels was found in all scaffolds, statistically significant higher amounts of OCN were detected in mineralized scaffolds obtained at 37 °C ($p < 0.05$) and 60 °C ($p < 0.01$) compared with the neat gelatin scaffold. Maximal OCN expression on most test scaffolds occurred on day 7, except for that on the scaffold obtained at 25 °C, but no significant difference was found in all the scaffolds. OCN levels were reduced on day 14 than seen on day 7, with the exception of cells grown on a scaffold obtained at 25 °C which show the significantly higher OCN than other scaffolds. The results indicate that cells attached to the scaffold containing a higher apatite content achieve a mature osteoblastic state more rapidly than on a scaffold with a lower apatite content.

Conclusions

In summary, we have developed a simple and rapid electrodeposition technique to fabricate mineralized porous scaffolds for bone regeneration. Both the surface topography and the chemical composition of the resulting apatite coating can be tailored by changing the electrodeposition parameters such as the deposition voltage, electrolyte temperature and ultrasonic field. A high-quality apatite coating can be achieved within a couple of hours by electrodeposition. Increasing the deposition voltage or electrolyte temperature favored the formation of large amounts of apatite coatings with compositions dominated by the hydroxyapatite crystals, whereas the presence of an ultrasonic field facilitated the production of homogeneous apatite coatings. Furthermore, the mineralized scaffolds demonstrated better support for cell proliferation and osteoblastic differentiation than a neat gelatin scaffold during the culture period, especially for the case of mineralized scaffolds by electrodeposition at 60 °C. Therefore, the method developed would be highly desired for the rapid mineralization of polymer scaffolds in which some biological molecules were loaded. Also, the mineralized gelatin scaffold with favorable pre-osteoblast growth and differentiation would make a promising scaffold material for bone regeneration.

Acknowledgements

This work was supported by the Natural Science Foundation of Shanghai (11ZR1400100), Doctoral Fund of Ministry of Education of China (200802551014), National Basic Research Program of China (2012CB933604), National Natural Science Foundation of China (81171707), Fundamental Research Funds for the Central Universities, Open Foundation of State Key Laboratory for Modification of Chemical Fibers and Polymer Materials (LK0804), and the Program of Introducing Talents of Discipline to Universities (B07024).

Notes and references

1 J. Venugopal, M. P. Prabhakaran, Y. Z. Zhang, S. Low, A. T. Choon and S. Ramakrishna, *Philos. Trans. R. Soc. London, Ser. A*, 2010, **368**, 2065–2081.
2 J. Y. Rho, L. Kuhn-Spearing and P. Zioupos, *Med. Eng. Phys.*, 1998, **20**, 92–102.
3 F. Z. Cui, Y. Li and J. Ge, *Mater. Sci. Eng., R*, 2007, **57**, 1–27.
4 P. Fratzl and R. Weinkamer, *Prog. Mater. Sci.*, 2007, **52**, 1263–1334.
5 S. E. Kim, H. W. Choi, H. J. Lee, J. H. Chang, J. Choi, K. J. Kim, H. J. Lim, Y. J. Jun and S. C. Lee, *J. Mater. Chem.*, 2008, **18**, 4994–5001.
6 T. G. Kim, S.-H. Park, H. J. Chung, D.-Y. Yang and T. G. Park, *J. Mater. Chem.*, 2010, **20**, 8927–8933.
7 S. S. Kim, M. S. Park, O. Jeon, C. Y. Choi and B. S. Kim, *Biomaterials*, 2006, **27**, 1399–1409.

8 W. Y. Choi, H. E. Kim, S. Y. Oh and Y. H. Koh, *Mater. Sci. Eng., C*, 2010, **30**, 777–780.
9 G. B. Cai, X. H. Guo and S. H. Yu, *Prog Chem.*, 2008, **20**, 1001–1014.
10 W. F. Zheng, W. Zhang and X. Y. Jiang, *Adv. Eng. Mater.*, 2010, **12**, B451–B466.
11 J. L. Chen, B. Chu and B. S. Hsiao, *J. Biomed. Mater. Res., Part A*, 2006, **79A**, 307–317.
12 P. X. Ma, *Adv. Drug Delivery Rev.*, 2008, **60**, 184–198.
13 C. L. He, G. Y. Xiao, X. B. Jin, C. H. Sun and P. X. Ma, *Adv. Funct. Mater.*, 2010, **20**, 3568–3576.
14 D. J. Blackwood and K. H. W. Seah, *J. Biomed. Mater. Res., Part A*, 2010, **93A**, 1551–1556.
15 R. Hu, C. J. Lin, H. Y. Shi and H. Wang, *Mater. Chem. Phys.*, 2009, **115**, 718–723.
16 J. H. Jang, O. Castano and H. W. Kim, *Adv. Drug Delivery Rev.*, 2009, **61**, 1065–1083.
17 F. Zhang, C. L. He, L. Cao, W. Feng, H. Wang, X. Mo and J. Wang, *Int. J. Biol. Macromol.*, 2011, **48**, 474–481.
18 M. I. Kay, R. A. Young and A. S. Posner, *Nature*, 1964, **204**, 1050–1052.
19 Q. Y. Zhang and Y. Leng, *Biomaterials*, 2005, **26**, 3853–3859.
20 C.-W. Yang and T.-S. Lui, *Acta Biomater.*, 2009, **5**, 2728–2737.
21 A. L. Oliveira, S. A. Costa, R. A. Sousa and R. L. Reis, *Acta Biomater.*, 2009, **5**, 1626–1638.
22 X. Lu, Z. F. Zhao and Y. Leng, *J. Cryst. Growth*, 2005, **284**, 506–516.
23 S. Mann, *Nature*, 1988, **332**, 119–124.
24 P. Calvert and S. Mann, *Nature*, 1997, **386**, 127–129.
25 P. X. Zhu, Y. Masuda and K. Koumoto, *Biomaterials*, 2004, **25**, 3915–3921.
26 Y. Tabata and Y. Ikada, *Biomaterials*, 1999, **20**, 2169–2175.
27 N. M. Alves, I. B. Leonor, H. S. Azevedo, R. L. Reis and J. F. Mano, *J. Mater. Chem.*, 2010, **20**, 2911–2921.
28 S. L. Chen, W. L. Liu, Z. J. Huang, X. G. Liu, Q. Y. Zhang and X. Lu, *Mater. Sci. Eng., C*, 2009, **29**, 108–114.
29 E. Agullo, J. Gonzalez-Garcia, E. Exposito, V. Montiel and A. Aldaz, *New J. Chem.*, 1999, **23**, 95–101.
30 R. Narayanan, T. Y. Kwon and K. H. Kim, *Mater. Sci. Eng., C*, 2008, **28**, 1265–1270.
31 I. Manjubala, I. Ponomarev, I. Wilke and K. D. Jandt, *J. Biomed. Mater. Res., Part B*, 2008, **84B**, 7–16.
32 M. Zandi, H. Mirzadeh, C. Mayer, H. Urch, M. B. Eslaminejad, F. Bagheri and H. Mivehchi, *J. Biomed. Mater. Res., Part A*, 2010, **92A**, 1244–1255.
33 R. Shu, R. McMullen, M. J. Baumann and L. R. McCabe, *J. Biomed. Mater. Res.*, 2003, **67A**, 1196–1204.
34 B. M. Whited, J. R. Whitney, M. C. Hofmann, Y. Xu and M. N. Rylander, *Biomaterials*, 2011, **32**, 2294–2304.
35 J. Hu, K. Feng, X. Liu and P. X. Ma, *Biomaterials*, 2009, **30**, 5061–5067.
36 M. Ngiam, S. Liao, A. J. Patil, Z. Cheng, C. K. Chan and S. Ramakrishna, *Bone*, 2009, **45**, 4–16.
37 L. Shor, S. Guceri, X. Wen, M. Gandhi and W. Sun, *Biomaterials*, 2007, **28**, 5291–5297.